AC RTN: Testing, Modelling, and Prediction

Kean H. Tok, Jian F. Zhang, James Brown, Zengliang Ye, Zhigang Ji, Weidong Zhang, and John S. Marsland

***Abstract*— Random Telegraph Noise (RTN) adversely induces time dependent device-to-device variations and requires modelling to optimize circuit design. Many early works were focused under DC test conditions, although digital circuits typically operate under AC conditions and it has been reported that AC RTN is substantially different from DC RTN. Tests on AC RTN were carried out mainly on individual traps and a reliable statistical distribution of trap time constants for AC RTN is still missing. This prevents verifying the statistical accuracy of Monte Carlo AC RTN simulation based on compact models, especially in terms of their ability to predict AC RTN as time window increases. Recently, an integral methodology has been proposed for DC RTN, which can not only model it at short time, but also predict it at long time. By introducing the concept of effective charged traps, the need for statistical distribution of trap time constants is removed, making RTN prediction similar to ageing prediction. The objectives of this work are to report statistical experimental AC RTN data and to test the applicability of integral methodology to them. For the first time, it will be shown that a model extracted from a time window of 7.8 s can be used to predict the statistical distribution of long term (3×10^4 sec) AC RTN. The dependence of AC RTN on frequency and time window is analyzed and the contributions of carrier tunneling from gate and substrate are assessed.**

***Index Terms*— Noise, Random telegraph noise (RTN), Jitters, Yield, Fluctuation, Device Variations, Time-dependent Variations.**

I. Introduction

RANDOM telegraph noise (RTN) in MOSFETs is caused by capturing a charge carrier from conduction channel and then giving it back [1]-[24]. It has attracted increasing amount of attentions recently, because of several reasons. First, the impact of a trapped charge increases as devices become smaller. Second, RTN is highly stochastic and induces a large time dependent device-to-device variation (DDV) and DDV has become a key issue for circuit design with nanoscale devices. Third, the need for low power consumption is driving operation voltage towards threshold, Vth, where a single trapped charge can have a large impact [1]-[5].

To assess the impact of RTN on circuits and to optimize their design, many efforts were made on both characterizing and modelling RTN [1]-[24]. On characterization, many early works were carried out under DC conditions [1],[6]-[15], although digital circuits typically operate under AC conditions. It has been reported that AC RTN is considerably different from DC RTN [16]-[19]. On modelling, works were carried out in both time [2]-[11],[16]-[19] and frequency [22] domain. In the time domain, Monte Carlo simulation has been carried out for both DC and AC RTN by assuming that RTN transitions are memoryless random Markov process [16]-[21]. The required inputs are the statistical distributions of (i) trap capture (τ_C)/emission (τ_E) time constants, (ii) RTN amplitude per trap, and (iii) number of traps per device. For AC RTN, τ_C and τ_E under both high ('H') gate bias Vg=Vdd and low ('L') Vg=0 are needed, which are represented by τ_{CH}, τ_{EH}, τ_{CL}, and τ_{EL}, hereafter.

It is widely accepted that the number of traps per device follows the Poisson's distribution [23],[24]. It has been proposed that trap amplitude can follow Exponential [5],[16],[23], Log-normal [1],[6],[16], or Generalized Extreme Value (GEV) distribution [7],[24]. The time constants have been assumed to follow either Log-normal [8],[9] or Log-uniform [1],[10],[11] distributions. When compared with the amplitude distribution, there are less data available to underpin the τ_C and τ_E distribution, as they are difficult to collect in large numbers even for DC RTN. For AC RTN, there are more challenges: as transistor is switched off under Vg=0, τ_{CL} and τ_{EL} cannot be measured directly.

Several methods were used to overcome the challenge and to obtain τ_{CL} and τ_{EL}. One of them is to assume that τ_{CL}/τ_{CH} and τ_{EH}/τ_{EL} is a constant, so that τ_{CL} and τ_{EL} can be estimated from the measured τ_{CH} and τ_{EH}, but the simulation results based on this assumption did not agree well with test data [8]. Another method uses compact models and τ_C and τ_E are assumed to be exponentially related to Ef-Et, where Ef is the Fermi-level at dielectric/substrate interface and Et is trap energy level [1],[3],[4],[19],[20]. Ef-Et under Vg=0 can be calculated and it can then be used to evaluate τ_{CL} and τ_{EL}. The problem is that the time constants obtained in this way are not verified by test data, so that the accuracy of these compact models for AC RTN simulation is typically not known.

To provide experimental data for AC RTN, the measured data under Vg=Vdd were joined together by removing the time of Vg=0 [17]. On one hand, it was reported that the τ_C measured in this way changes little from its DC value. As τ_{CL} is typically much larger than τ_{CH}, the duration of Vg=0 contributes little to trap capture and its removal has little effects on capture. On the other hand, τ_{EL} is typically smaller than τ_{EH}, so that the time under Vg=0 can reduce the measured τ_E. By measuring both τ_C and τ_E under Vg=Vdd and removing the Vg=0 duration, the AC

Manuscript received MM DD, YYYY. This work was supported by the Engineering and Physical Science Research Council of UK under the grant no. EP/T026022/1. The review of this paper was arranged by Editor Edmundo Gutiérrez-D (Corresponding author: J. F. Zhang, e-mail: j.f.zhang@ljmu.ac.uk)

K. H. Tok, J. F. Zhang, J. Brown, Z. Ye, Z. Ji, W. Zhang, and J. S. Marsland are with School of Engineering, Liverpool John Moores University, Liverpool L3 3AF, UK. Z. Ji now is with School of Microelectronics, Shanghai Jiaotong University, Shanghai 200240, China.

RTN of individual traps has been modelled successfully [16]-[19]. At present, however, there is a lack of reliable statistical distribution of the τ_C and τ_E measured in this way. As a result, the statistical accuracy of Monte Carlo modelling for AC RTN remains to be verified for multiple traps and devices in real circuits, especially in term of its capability to predict the AC RTN beyond the test time window.

The objectives of this work are threefold: to provide statistical AC RTN data at device level, rather than single trap; to develop a model for AC RTN, that can not only fit test data, but also predict the long term AC RTN; and to analyze test data and simulation results, leading to an improved understanding of AC RTN. Unlike the early works that focus on individual traps [17]-[19], AC RTN data with time window up to 3×10^4 sec are collected on device level that can have multiple traps.

Recently, an integral methodology has been proposed and used to model DC RTN [24]. The applicability of this methodology to AC RTN will be tested in this work. The dependence of AC RTN on frequency and time window will be analyzed. Both acceptor-like and donor-like traps are modelled and their differences in carrier tunneling will be studied.

II. Devices and Experiments

A. Devices

nMOSFETs fabricated by a 28 nm CMOS process were used in this work. The channel width and length are 90 nm and 27 nm, respectively. The gate dielectric consists of a stack of a Hf-high-k layer and an interfacial SiON layer with an equivalent oxide thickness of 1.2 nm. The devices were arranged in arrays and each of them is assessed through address codes. The average threshold voltage, Vth, is 0.45 V.

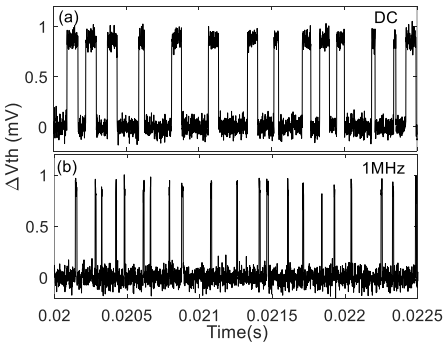

Fig. 1. An example of measured data for a device with one acceptor-like trap. Vg is under DC (a) and 1 MHz (b). The duration of Vg=0 was removed in (b).

B. Experiments

The tests were carried out with Vg alternating between 0.5 V and 0 V under a constant drain bias of 0.1 V. The top Vg is chosen to be close to Vth to make the test relevant to low power operation, where RTN can be profound [7],[10],[24]. The frequency of Vg is in a range of 100 Hz to 1 MHz with a duty cycle of 50%. Temperature is 125 °C. To enable statistical analysis, 402 devices were tested for a relatively short time window of 7.8 sec (time after removing Vg=0 duration). To verify that the AC RTN model extracted from data in this short window can be used to predict long term RTN, tests with a time window up to 3×10^4 sec were also carried out for 60 devices.

Before RTN test, a pulse (3 μs) Id-Vg was measured. During RTN tests, drain current, Id, was monitored continuously at a sampling rate of 1 Mpoint/sec [25]. The reference Id, Iref, was obtained from the average of the first 10 points and the threshold voltage shift is evaluated from ΔVth=(Iref-Id)/gm, where gm is the transconductance obtained from the pulse Id-Vg for each device at Vg=0.5 V [24].

III. Results and Discussions

A. AC RTN data at device level

When there is only one trap in a device, Figs. 1(a) and 1(b) compares the DC and AC RTN. Following the earlier works [17]-[19], the duration of Vg=0 was removed in Fig. 1(b). We will use the term of 'time' or 'time window' for the cumulative time under Vg=0.5 V, hereafter. For a duty cycle of 50%, the actual AC RTN test time doubles the 'time window'. Under AC, the trap in Fig. 1 spends more time at the low level of ΔVth and there are more transitions between the two levels, in agreement with early work [17]. The result supports that this trap is acceptor-like, which captures an electron and induces a positive ΔVth. Because emission under Vg=0 is more efficient, the trap can only hold the electron for short time at the high level of ΔVth in Fig. 1(b).

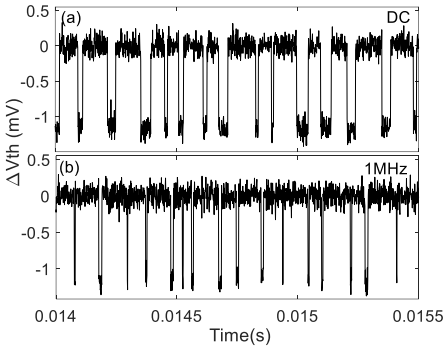

Fig. 2. An example of measured data for a device with one donor-like trap. Vg is under DC (a) and 1 MHz (b). The duration of Vg=0 was removed in (b).

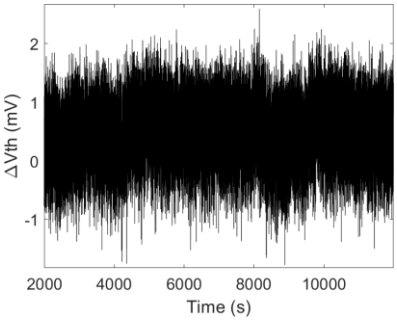

Fig. 3. An example of complex RTN over a long time window.

The positive ΔVth in Figs. 1(a) and 1(b) corresponds to a reduction of drain current, Id. An increase of Id was also often observed, which lead to a negative ΔVth, as shown in Figs. 2(a) and 2(b). This negative ΔVth can come from either charging a donor-like trap positively or emitting an electron from a prefilled acceptor-like trap. Following early work [24], we use the term 'donor-like trap' to represent ΔVth<0, hereafter. For AC RTN, Fig. 2(b) confirms that the emission of positive charge, i.e. capturing an electron and becoming neutral, is also more efficient under Vg=0.

The devices in Figs. 1 and 2 only have one active trap within the measurement window. The trap time constant in this case can be readily extracted and used for Monte Carlo simulation. Many devices, however, do not have such clear RTN signal. As time window increases, the number of active traps in a device increases, resulting in complex fluctuation and one example is given in Fig. 3. It is difficult to extract time constants of individual traps in this case. An integral methodology has been proposed to overcome this challenge [24] and will be briefly described next.

B. Integral methodology

This method uses the ΔVth measured at device level as inputs and does not require experimentally separating ΔVth into contributions of individual traps. As a result, it does not require one device having only one trap and is applicable to devices with any number of traps. At a given time, ΔVth measured from multiple devices were grouped together to form a dataset and their cumulative distribution function (CDF) is given in Fig. 4. The concept of 'Effective Charged Traps (ECT)" is introduced, which assume that this CDF comes from a set of traps that are always charged. In this way, the burden for finding the statistical distribution of trap time constants is removed, greatly simplifying the testing and analysis.

The next step is to extract the number of ECT that can reproduce a given CDF of ΔVth. By assuming the number of traps per device follows the Poisson's distribution and selecting a RTN amplitude distribution, such as Exponential, Log-normal, or GEV, the average number of ECT per device can be extracted by the maximum likelihood estimation for both acceptor-like (N_A) and donor-like (N_D) traps [24].

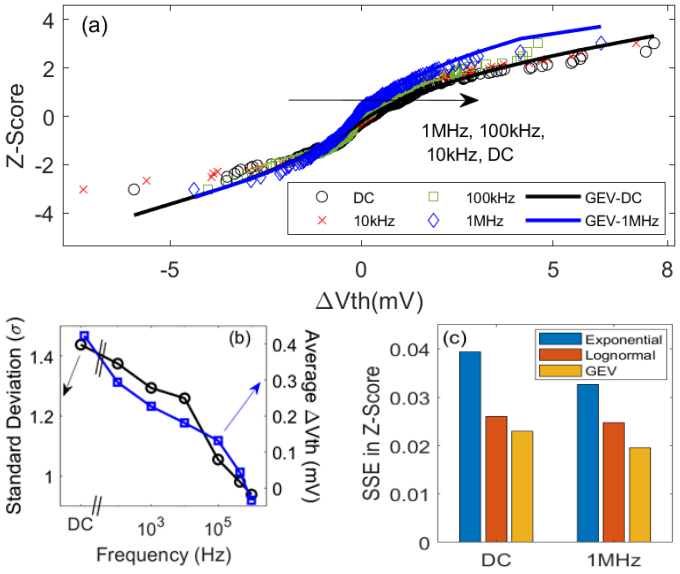

Fig. 4. (a) The Cumulative Distribution (CD) of test data (symbols). The lines are fitted function with GEV for DC (black) and 1 MHz (blue). (b) Dependance of standard deviation (σ) and mean ΔVth on frequency. (c) A comparison of the sum of squared error (SSE) per device of the CDF extracted for DC and 1 MHz RTN. The RTN amplitude distribution per trap is assumed to follow Exponential, Log-normal, and GEV, respectively. The time window is 7.8 s.

The above process for extracting N_A and N_D is repeated for different time window. Longer time window covers slower traps and increases |ΔVth|, which in turn results in larger N_A and N_D. The N_A and N_D versus time obtained in this way can be used to extract their kinetics. For DC RTN, it has been shown that this kinetics can be used to predict N_A and N_D at longer time [24]. Once N_A and N_D are known, the probability for a device to have a specific ΔVth can be calculated.

Table I. The pdf formula and their extracted parameter values. δVth is the threshold voltage shift per trap.

	PDF of δVth	Acceptor	Donor
Exponential	$\frac{1}{\eta}e^{-\frac{\delta Vth}{\eta}}$	$\eta = 0.54$	$\eta = 0.49$
Lognormal	$\frac{1}{\delta Vth\theta\sqrt{2\pi}}e^{\left(-\frac{(\ln(\delta Vth)-\epsilon)^2}{2\theta^2}\right)}$	$\epsilon = -0.37$ $\theta = 0.14$	$\epsilon = -0.64$ $\theta = 0.16$
GEV	$\frac{1}{\beta}(k)^{\xi+1}e^{-k}$ $k = \left(1+\xi\left(\frac{\delta Vth-\alpha}{\beta}\right)\right)^{-\frac{1}{\xi}}$	$\xi = 0.32$ $\alpha = 0.41$ $\beta = 0.36$	$\xi = 0.36$ $\alpha = 0.29$ $\beta = 0.23$
Thermal	$\frac{1}{\sigma\sqrt{2\pi}}e^{-\frac{1}{2}\left(\frac{\Delta Vth}{\sigma}\right)^2}$	$Exponential, \sigma = 0.09$ $Lognormal, \sigma = 0.13$ $GEV, \sigma = 0.11$	

C. Applicability of Integral methodology to AC RTN

ΔVth under different frequencies is compared in Figs. 4(a) and 4(b). ΔVth, its mean value and standard deviation is smaller for AC RTN, because of the enhanced emission during Vg=0. As a result, the RTN under AC operation cannot be modeled from DC RTN data and AC measurements have to be carried out. Since ΔVth can be either positive or negative, its mean value (<1 mV) is much smaller than its standard deviation.

The lines in Fig. 4(a) are the fitted cumulative distribution function (CDF). Their corresponding probability distribution function (PDF) and the extracted model parameters are given in Table I. Fig. 4(c) shows that the error for AC is not larger than that for DC. As a result, it is concluded that the integral method is equally applicable for AC RTN. This is understandable: AC mainly impacts emission, but the integral methodology assumes CDF originating from ECT that are always charged and detailed emission process is not needed here.

The results in Fig. 4 were obtained for a time window of 7.8 s. The same procedure is applied for other time windows between 10^{-4} s and 7.8 s and the extracted N_A and N_D are given in Fig. 5 for Exponential, Log-normal, and GEV RTN amplitude distributions. As expected, both N_A and N_D increased with time window, but decreased for higher frequency due to reduced trap occupancy.

Fig. 6 gives the extracted average threshold voltage shift per trap, μ. Unlike the N_A and N_D in Fig. 5, μ is insensitive to frequency. This is because that the same traps are responsible for AC and DC RTN. Although AC enhances emission, it does not change RTN amplitude, as shown in Figs. 1 and 2.

The N_A and N_D versus time in Fig. 5 can be used to extract their kinetics. Three different kinetics were tested: power law, scaled Log-normal CDF, and Log-uniform [24]. Fig. 5 shows that all three can fit the data reasonably well within the short time window of 7.8 s. One powerful feature of the integral methodology is that these kinetics can be extrapolated to longer time window to predict the long term DC RTN [24], making RTN prediction similar to predicting ageing induced by bias temperature instabilities [26],[27] and hot carriers [28]. The prediction capability for AC RTN will be tested next.

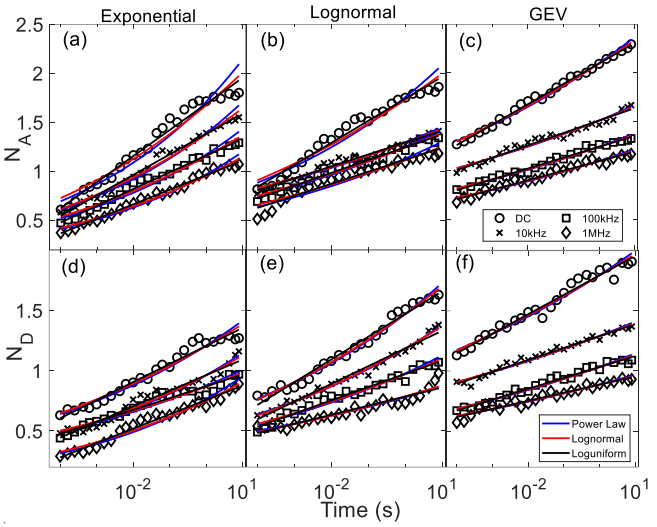

Fig. 5. Dependence of average number of ECT per device on time window (symbols) at different frequencies. N_A in the top row (a,b,c) is for acceptor-like traps with Exponential, Log-normal, and GEV distributions, respectively. N_D in the bottom row (d,e,f) is for donor-like traps. The lines are fitted kinetics with Power law (blue), scaled Log-normal CDF (red), and Log-uniform (black).

Fig. 7 gives the N_A and N_D for AC RTN measured up to a time window of 3×10^4 sec. The three kinetics extracted from the data within 7.8 s is extrapolated and compared with the test data. The differences between predictions by the three kinetics can be considerable and some kinetics clearly agrees better with the test data. To make a quantitative comparison, Fig. 8 gives the errors between predictions and test data. When RTN amplitude is assumed to follow Exponential and Log-normal distribution, the scaled Log-normal CDF kinetics give lower errors. The lowest error, i.e. the best fit, however, is obtained for GEV with Log-uniform kinetics.

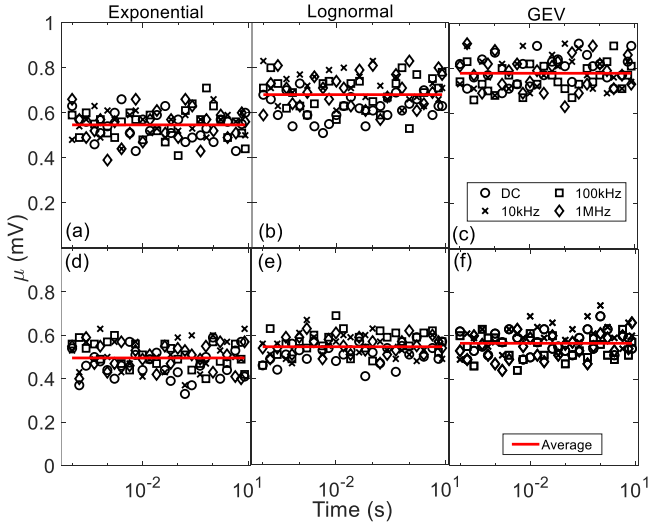

Fig. 6. The extracted average δVth per trap, μ, for DC and AC RTN at different frequencies. Solid lines are the mean values of all data. (a,b,c) are acceptor-like traps and (d,e,f) are donor-like traps.

We now investigate how well the N_A and N_D predicted in Fig. 7 can be used to evaluate the CDF at an AC time window of 3×10^4 sec. Figs. 9(a) and 9(b) compares the CDF calculated from the predicted N_A and N_D with the measured one and good agreement has been obtained. Fig. 9(c) shows that the prediction error for AC RTN is similar to that for DC RTN. As a result, the integral methodology can be used to extract a model from 7.8 s tests that is capable to predict AC RTN at 3×10^4 sec, over three orders of magnitude ahead in time.

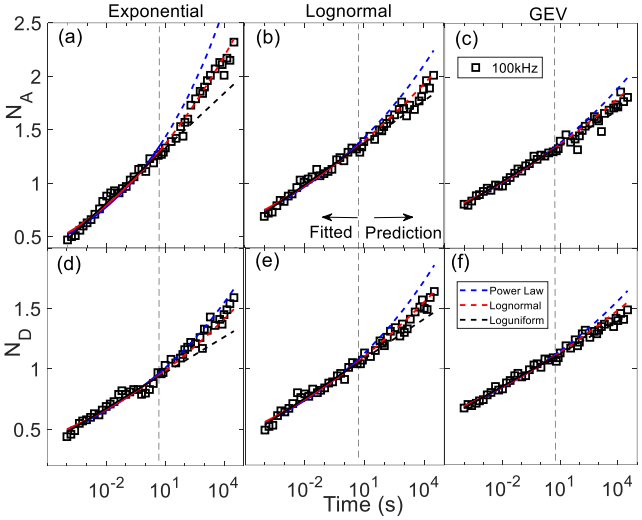

Fig. 7. Prediction of the average number of acceptor-like traps, N_A, in the top row (a, b, c) and donor-like traps, N_D, in the bottom row (d, e, f) for AC RTN at 100 kHz. Symbols are extracted by fitting the δVth distributions (Exponential, Lognormal, and GEV). The solid lines within 7.8 s are the fitted kinetics with Power law (blue), Log-normal (red), and Log-uniform (black). The dashed lines beyond 7.8 s are extrapolated from the solid lines. The symbols beyond 7.8 s were not used for fitting.

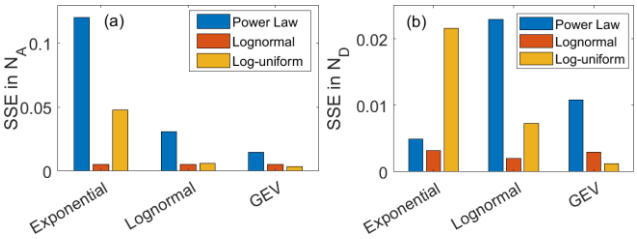

Fig. 8. The sum of squared errors per device of the prediction in Fig. 7 for acceptor-like (a) and donor-like (b) average number of traps per device. The lowest errors were obtained for Log-uniform kinetic with GEV δVth distribution.

A comparison of Fig. 4(a) with Fig. 9(a) shows that their ΔVth has similar range. Figs. 4(a) and 9(a) were obtained for a time window of 7.8 and 3×10^4 s, respectively. One would expect that Fig. 9(a) should have a larger ΔVth range, as larger time window allows slower traps to be included. This apparent discrepancy originates from the difference in number of samples used: 402 for Fig. 4(a) and 60 for Fig. 9(a). A larger number of samples has more chances of capturing rare event and, in turn, increases the statistical range. This compensates the effect of smaller time window.

D. Analysis of AC RTN

Fig. 10 shows N_A(AC)/N_A(DC) and N_D(AC)/N_D(DC) against time window. The main feature is that they decrease relatively fast with time initially and then more slowly for longer time window. For a given trap, its emission time follows [1],[3],[4],[19],[20],

$$\tau_E \propto \exp\left(\frac{Ef-Et}{kT}\right). \qquad (1)$$

At a given distance from the interface, a trap with its energy level Et further below Ef will have larger τ_E. When Vg is switched from Vdd to zero for AC RTN, it shifts (Ef-Et) by the same amount for traps of different Et. This means τ_{EL}/τ_{EH} should be same for fast and slow traps, so that one may expect $N_A(AC)/N_A(DC)$ to be independent of time window, against the observed reduction in Fig. 10. To understand the reduction in Fig. 10, we examine the impact of frequency on τ_E next.

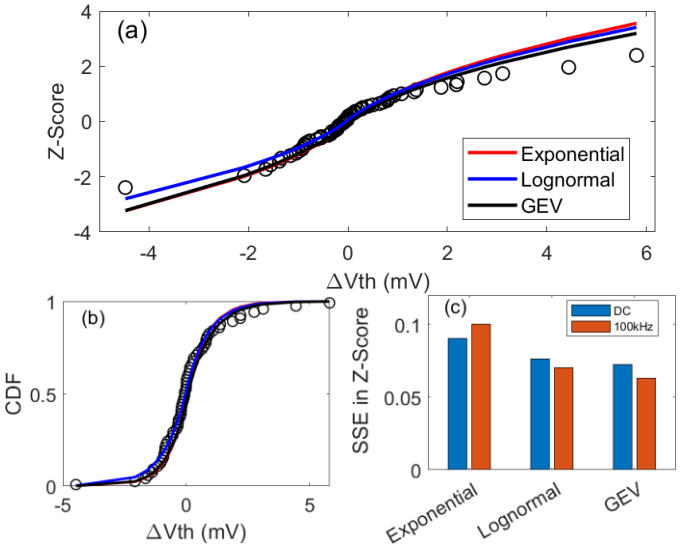

Fig. 9. AC (100 kHz) RTN prediction for the CDF of ΔVth at the time window of 3×10^4 s by the model extracted from test data within 7.8 s. Symbols are the measured data and the lines are the calculated CDF by using the predicted N_A and N_D in Fig. 7 and the average μ in Fig. 6, based on different δVth distributions. The CDF is plotted in Z-score (a) and linearly in (b). (c) compares the errors of DC and AC predictions and shows that the smallest error was obtained for Log-uniform kinetic with GEV δVth distribution.

When there is only one active trap in a device, like that in Figs. 1 and 2, its τ_C and τ_E can be readily extracted and one example for acceptor-like and donor-like trap is given in Fig. 11(a) and 11(b), respectively. In agreement with early work [16]-[19], τ_C is independent of frequency, f, because $\tau_{CL}>>\tau_{CH}$ and removing the Vg=0 durations have little impact on capture.

Although τ_{EH} and τ_{EL} are determined by (Ef-Et) and should be independent of frequency, the τ_E measured at Vdd in Figs. 1(b) and 2(b) is neither τ_{EH} nor τ_{EL} and Fig. 11 shows that it can depend on frequency, in agreement with early work [16]-[19]. The dependence of τ_E on frequency can be divided into three regions. At low frequency Region 1 (R1) in Fig. 11, τ_E is insensitive to frequency. In Region 2 (R2), τ_E reduces for higher frequency. Finally, in high frequency Region 3 (R3), τ_E becomes insensitive to frequency again. A physical interpretation for this dependence will be given below.

In the inset of Fig. 11(a), t_H=1/(2f) is half of the AC period under Vg=0.5 V. The number of RTN transition during t_H, n, is:

$$n = \frac{2t_H}{\tau_{CH} + \tau_{EH}}, \qquad (2)$$

In R1, f is low enough to make $t_H>>(\tau_{CH}+\tau_{EH})$. There are many RTN transitions within t_H, i.e n>>1. During Vg=0, $t_L>>\tau_{EL}$, but when t_L is removed by joining the two dots in Fig. 11(a) together, the number of emission will be increased by a maximum of 1 to (n+1)≈n, so that the measured $\tau_E\approx\tau_{EH}$, which is hardly affected by Vg=0 duration and independent of frequency here.

As frequency increases and t_H reduces in R2, n approaches 1. If $t_L>>\tau_{EL}$, trapped charge will be emitted during t_L and the number of emission during one AC period is (n+1)>n. The emission during t_L reduces the measured τ_E. When n<<1, (n+1)≈1, the measured τ_E now is controlled by frequency and does not equal to τ_{EH}. An increase of frequency reduces t_L and in turn τ_E.

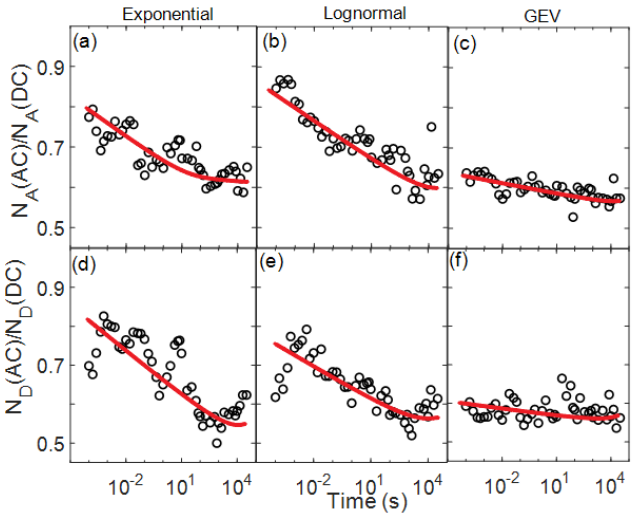

Fig. 10. AC (100 kHz) RTN against DC RTN ratio from 10^{-4} to $3x10^4$ s for acceptor-like traps, N_A, in the top row (a, b, c) and donor-like traps, N_D, in the bottom row (d, e, f). The red lines are eye guides, showing that the reduction trend slows down at longer time.

Finally, when frequency is high enough to make $t_L<<\tau_{EL}<\tau_{EH}$, we enter R3 where emission happens during both t_H and t_L to give,

$$\tau_E = \frac{\tau_{EH}\tau_{EL}}{\tau_{EH} + \tau_{EL}}. \qquad (3)$$

τ_E now is independent of frequency again. If $\tau_{EL}<<\tau_{EH}$, $\tau_E\approx\tau_{EL}$, i.e. although the measurement is at Vg=Vdd, the measured τ_E is actually the emission time at Vg=0.

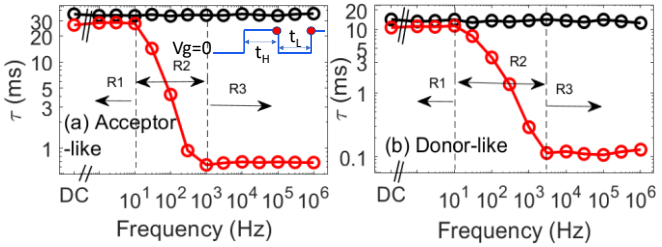

Fig. 11. Time constants, τ, versus frequency for single acceptor-like trap (a) and donor-like trap (b). The red and black symbols are emission (τ_E) and capture (τ_C) time, respectively. R1, R2, and R3 are the three regions for the emission time.

We now use Fig. 11 to explain the results in Fig. 10. When time window is small, active traps are fast and they can be either in R1 or close to the top of R2, where AC reduces τ_E modestly, resulting in a relatively large $N_A(AC)/N_A(DC)$ in Fig. 10. As time increases, slower traps become active and they are in R2, where AC causes an increasingly larger reduction of τ_E, leading to the reduction of $N_A(AC)/N_A(DC)$. As time increases further, the new active traps are slow enough to be in R3, where the impact of AC

on τ_E stabilizes, so that $N_A(AC)/N_A(DC)$ only decreases slowly with time here.

The test facilities used in this work only allows reliable measurement to be made up to 1 MHz. There are traps that are too fast to make $t_L \ll \tau_{EL}$ even at 1 MHz, so that they do not enter R3. Examples of this case are given in Fig. 12(a) and 12(b) for acceptor-like and donor-like traps, respectively. This explains the continuous reduction of N_A and N_D with frequency in Fig. 13.

We now use the AC RTN to study the difference in tunneling process between acceptor-like and donor-like traps. For acceptor-like traps, emission will be more efficient under Vg=0, if electron is emitted to the substrate, as illustrated in Fig. 14a. The enhanced emission of AC RTN supports the tunneling is between traps and substrate, therefore.

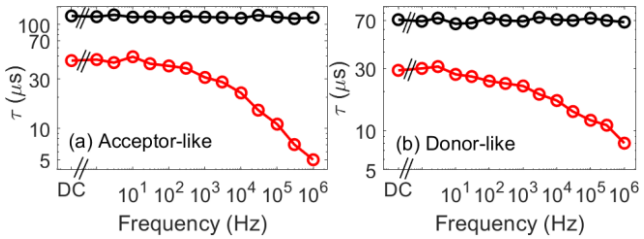

Fig. 12. Time constant, τ, versus frequencies for single acceptor-like trap (a) and donor-like trap (b). In contrast with Fig. 11, the emission time does not enter into region R3 even at 1 MHz here.

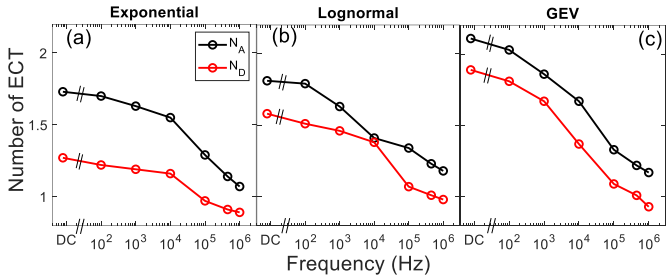

Fig. 13. Dependence of the extracted N_A (black) and N_D (red) at 7.8 s on frequency. (a,b,c) uses Exponential, Log-normal, and GEV δVth distribution, respectively.

For donor-like traps, AC also enhances the emission, as shown in Figs. 2(b), 11(b) and 12(b). To neutralize the positive charge or to restore the pre-trapped electron, an electron must tunnel to the trap. If this electron comes from the substrate, it should be less efficient under Vg=0 than under Vg=+0.5 V, which disagrees with enhanced emission under AC. On the other hand, electron tunneling to the trap is more efficient under Vg=0, if it is from gate, as illustrated in Fig. 14b. As a result, acceptor-like and donor-like traps should be dominated by tunneling from substrate and gate, respectively. For a given time window, one may also expect that active donor-like traps are closer to the gate. This is supported by the smaller average impact per donor-like trap in Fig. 6. On the relative tunneling from gate against that from substrate, Figs. 14(c) and 14(d) shows N_D/N_A is around 0.8 and insensitive to either time or frequency.

IV. CONCLUSIONS

Unlike early works that focused on individual traps, this work reports statistical experimental data for AC RTN at device level with time window up to 3×10^4 sec. The ΔVth measured from multiple devices were grouped together to form a data set and it is found that the integral methodology is equally applicable to AC RTN as to DC RTN. At a given time, the CDF of ΔVth is used to extract the number of effective charged acceptor-like and donor-like traps through the maximum likelihood estimation. The N_A and N_D obtained from data within a time window of 7.8 s is used to extract their kinetics. For the first time, it is shown that these kinetics can predict the N_A and N_D at 3×10^4 sec, a factor of 3,846 ahead in time. The CDF evaluated from the predicted N_A and N_D agrees well with test data. If one assumes that N_A and N_D kinetics extracted from a test time of one day can predict the AC RTN by the same factor of 3,846 ahead, it will cover a time range over 10 years. The dependence of AC RTN on time window and frequency is analyzed and RTN still reduces with frequency at 1 MHz, indicating there are traps with an emission time under Vg=0 less than 1 μs. The AC RTN data support that there are substantial tunneling activities between traps and both gate and substrate.

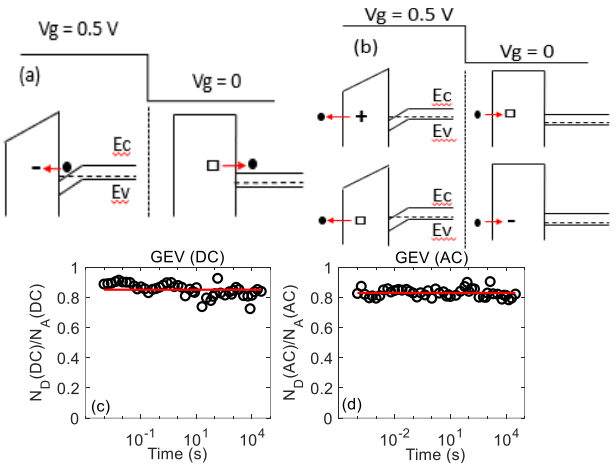

Fig. 14. A schematic illustration of carrier tunneling for acceptor-like trap (a) and donor-like trap (b) to explain the AC-enhanced emission. N_D/N_A is independent of time for both DC (c) and AC (d) RTN. ●, -, +, and □ represents electron, trapped negative, trapped positive charges, and neutral traps, respectively.

ACKNOWLEDGMENT

The authors thank D. Vigar of Qualcomm Technologies International Ltd for supplying test samples.

REFERENCES

[1]. M. J. Kirton and M. J. Uren, "Noise in solid-state microstructures: A new perspective on individual defects, interface states and low-frequency (1/*f*) noise", *Advances in Physics*, vol. 38, no. 4, pp. 367-468, 1989, doi: 10.1080/00018738900101122.

[2]. A. Asenov, R. Balasubramaniam, A.R. Brown, J.H. Davies "RTS amplitudes in decananometer MOSFETs: A 3D simulation study," *IEEE Trans. Electron Devices*, vol. 50, no. 3, pp. 839-845, 2003, doi: 10.1109/TED.2003.811418.

[3]. T. Grasser, "Stochastic charge trapping in oxides: From random telegraph noise to bias temperature instabilities," *Microelectron. Rel.*, vol. 52, pp. 39-70, 2012, doi:10.1016/j.microrel.2011.09.002.

[4]. T. Grasser, H. Reisinger, P.-J. Wagner, F. Schanovsky, W. Goes, B. Kaczer, "The Time Dependent Defect Spectroscopy (TDDS) for the Characterization of the Bias Temperature Instability," *IEEE Proc. Int. Rel. Phys. Symp. (IRPS)*, May 2010, pp. 16–25, doi: 10.1109/IRPS.2010.5488859.

[5]. B. Kaczer *et al.*, "Origin of NBTI variability in deeply scaled pFETs," in *IEEE Proc. Int. Rel. Phys. Symp. (IRPS)*, May 2010, pp. 26–32, doi: 10.1109/IRPS.2010.5488856.

[6]. K. Sonoda, K. Ishikawa, T. Eimori, O. Tsuchiya, "Discrete Dopant Effects on Statistical Variation of Random Telegraph Signal Magnitude," *IEEE Trans. Electron Devices*, vol. 54, no. 8, pp.1981-1925, 2017, doi: 10.1109/TED.2007.900684.

[7]. M. Mehedi *et al.*, "On the accuracy in modelling the statistical distribution of Random Telegraph Noise Amplitude," *IEEE Access*, vol. 9, pp.43551-43561, 2021, doi: 10.1109/ACCESS.2021.3065869.

[8]. K. Ito, T. Matsumoto, S. Nishizawa, H. Sunagawa, K. Kobayashi, H. Onodera, "Modeling of Random Telegraph Noise under Circuit Operation-Simulation and Measurement of RTN-induced delay fluctuation," in *Proc. 12th Int'l Symp. on Quality Electronic Design*, pp.22-27, 2011, doi: 10.1109/ISQED.2011.5770698.

[9]. M. Tanizawa *et al.*, "Application of a Statistical Compact Model for Random Telegraph Noise to Scaled-SRAM Vmin Analysis," in *Proc. Symp. VLSI Technol.*, Jun. 2010, pp. 95–96, doi: 10.1109/VLSIT.2010.5556184.

[10]. M. Mehedi *et al.*, "An assessment of the statistical distribution of Random Telegraph Noise Time Constants," *IEEE Access*, vol. 8, no. 10, pp.1496-1499, 2020, doi: 10.1109/ACCESS.2020.3028747.

[11]. M. Duan *et al.*, "Time-dependent variation: A new defect-based prediction methodology," in *Proc. Symp. Very Large Scale Integr. (VLSI) Technol.*, Jun. 2014, pp. 74–75.

[12]. H. Miki *et al.*, "Understanding Short-term BTI Behavior through Comprehensive Observation of Gate-voltage Dependence of RTN in Highly Scaled High-k / Metal-gate pFETs," in *Proc. Symp. Very Large Scale Integr. (VLSI) Technol.*, Jun. 2011, pp. 148–149.

[13]. T. Nagumo, K. Takeuchi, T. Hase, and Y. Hayashi, "Statistical Characterization of Trap Position, Energy, Amplitude and Time Constants by RTN Measurement of Multiple Individual Traps," in *IEDM Tech. Dig.*, Dec. 2010, pp. 628–631, doi: 10.1109/IEDM.2010.5703437.

[14]. A. Manut *et al.*, "Trigger-When-Charged: A Technique for Directly Measuring RTN and BTI-Induced Threshold Voltage Fluctuation Under Use-Vdd," *IEEE Trans. Electron Devices*, vol. 66, no.3, pp. 1482-1488, 2019, doi: 10.1109/TED.2019.2895700.

[15]. M. Duan *et al.*, "New analysis method for time-dependent device-to-device variation accounting for within-device fluctuation," *IEEE Trans. Electron Devices*, vol. 60, no. 8, pp. 2505–2511, Aug. 2013, doi: 10.1109/TED.2013.2270893.

[16]. R. Wang *et al.*, "Too Noisy at the Bottom? -Random Telegraph Noise (RTN) in Advanced Logic Devices and Circuits," in *IEDM Tech. Dig.*, Dec. 2018, pp. 388–391, doi: 10.1109/IEDM.2018.8614594.

[17]. J. Zou *et al.*, "New insights into AC RTN in scaled high-k/metalgate MOSFETs under digital circuit operations," in *Proc. Symp. VLSI Technol. (VLSI)*, Jun. 2012, pp. 139–140. Doi: 10.1109/VLSIT.2012.6242500.

[18]. J. Zou *et al.*, "Deep understanding of AC RTN in MuGFETs through new characterization method and impacts on logic circuits," *in Proc. VLSI Symp. Technol. (VLSIT)*, Jun. 2013, pp. T186–T187.

[19]. M. Luo, R. Wang, S. Guo, J. Wang, J. Zou, and R. Huang, "Impacts of Random Telegraph Noise (RTN) on Digital Circuits," *IEEE Trans. Electron Devices*, vol. 62, no. 6, pp. 1725-1732, 2015, doi: 10.1109/TED.2014.2368191.

[20]. P. Weckx *et al.*, "Defect-based compact modeling for RTN and BTI variability," in *Proc. Int. Rel. Phys. Symp.*, 2017, pp. CR-7.1-CR-7.6.

[21]. R. Gao *et al.*, "A fast and test-proven methodology of assessing RTN/fluctuation on deeply scaled nano pMOSFETs," in *Proc. Int. Rel. Phys. Symp. (IRPS)*, 2020.

[22]. A. J. Scholten, L.F. Tiemeijer, R. van Langevelde, R.J. Havens, A.T.A. Zegers-van Duijnhoven, V.C. Venezia, "Noise Modeling for RF CMOS Circuit Simulation", *IEEE Trans. Electron Devices*, vol. 50, no. 3, pp. 618–632, 2003, doi: 10.1109/TED.2003.810480.

[23]. M. Toledano-Luque *et al.*, "From mean values to distributions of BTI lifetime of deeply scaled FETs through atomistic understanding of the degradation," in *Proc. Symp. Very Large Scale Integr. (VLSI) Technol.*, Jun. 2011, pp. 152–153.

[24]. K. H. Tok *et al.*, "An Integral Methodology for Predicting Long-Term RTN," in *IEEE Transactions on Electron Devices*, vol. 69, no. 7, pp. 3869–3875, July 2022. doi: 10.1109/TED.2022.3176585.

[25]. M. Duan *et al.*, "Key issues and techniques for characterizing time dependent device-to-device variation of SRAM," in *IEDM Tech. Dig.*, Dec. 2013, pp. 31.3.1–31.3.4, doi: 10.1109/IEDM.2013.6724730.

[26]. R. Gao *et al.*, "Reliable time exponents for long term prediction of negative bias temperature instability by extrapolation," *IEEE Trans. Elec. Dev.*, Vol. 64, pp. 1467-1473, 2017, doi: 10.1109/TED.2017.2669644.

[27]. J. F. Zhang, Z. Ji, W. Zhang, "As-grown-generation (AG) model of NBTI: A shift from fitting test data to prediction," *Microelectron. Rel.*, vol. 80, pp. 109-123, 2018, doi: /10.1016/j.microrel.2017.11.026.

[28]. M. Duan, J. F. Zhang, Z. Ji, W. Zhang, B. Kaczer, and A. Asenov, "Key Issues and Solutions for Characterizing Hot Carrier Aging of Nanometer Scale nMOSFETs," *IEEE Trans. Electron Devices*, vol. 64, no.6, pp. 2478-2484, 2017, doi: 10.1109/TED.2017.2691008.